2CFastICA: A Novel Method for High Density Surface EMG Decomposition Based on Kernel Constrained FastICA and Correlation Constrained FastICA

Maoqi Chen and Ping Zhou, *Senior Member, IEEE*

***Abstract*— This study presents a novel high density surface electromyography (EMG) decomposition method, named as 2CFastICA, because it incorporates two key algorithms: kernel constrained FastICA and correlation constrained FastICA. The former focuses on overcoming the local convergence of FastICA without requiring the peel-off strategy used in the progressive FastICA peel-off (PFP) framework. The latter further refines the output of kernel constrained FastICA by correcting possible erroneous or missed spikes. The two constrained FastICA algorithms supplement each other to warrant the decomposition performance. The 2CFastICA method was validated using simulated surface EMG signals with different motor unit numbers and signal to noise ratios (SNRs). Two source validation was also performed by simultaneous high density surface EMG and intramuscular EMG recordings, showing a matching rate (MR) of (97.2 ± 3.5)% for 170 common motor units. In addition, a different form of two source validation was also conducted taking advantages of the high density surface EMG characteristics of patients with amyotrophic lateral sclerosis, showing a MR of (99.4 ± 0.9)% for 34 common motor units from interference and sparse datasets. Both simulation and experimental results indicate that 2CFastICA can achieve similar decomposition performance to PFP. However, the efficiency of decomposition can be greatly improved by 2CFastICA since the complex signal processing procedures associated with the peel-off strategy are not required any more. Along with this paper, we also provide the MATLAB open source code of 2CFastICA for high density surface EMG decomposition.**

***Index Terms*— FastICA, kernel constrained FastICA, correlation constrained FastICA, high density surface EMG, decomposition, two source validation, open source code.**

I. Introduction

IN RECENT decades, high density surface electromyography (EMG) decomposition has undergone significant growth. Among various algorithms and methods being reported for high density surface EMG decomposition, two of them have attracted considerable attention. One is the convolution kernel compensation (CKC) method proposed by Holobar and Zazula [1], [2], which describes high density surface EMG signal using a convolution model and realizes its decomposition by compensating channel responses and reconstructing the motor unit pulse trains directly. The other is the progressive FastICA peel-off (PFP) method proposed by Chen et al. [3], [4], which is a novel deflationary EMG decomposition framework based on FastICA [5]. Since then, FastICA is generally recognized as a useful approach, readily adapted and applied for high density surface EMG decomposition. For example, a decomposition framework combining FastICA and CKC was proposed right after the PFP [6]. A range of other forms of high density surface EMG decomposition methods have also been reported, with either CKC or FastICA as key elements [7], [8], [9], [10], [11], [12], [13], [14], [15], [16], [17], [18], [19].

A key problem or difficulty of applying FastICA for high density surface EMG decomposition is how to address the local convergence of FastICA, given that FastICA tends to converge on the firing trains of only a few motor units, thus compromising the decomposition yield and efficiency. Although orthogonalization has been utilized in FastICA to estimate different source signals, it is insufficient to solve the problem of local convergence in high density surface EMG decomposition scenarios.

To overcome the local convergence problem, our previous study has designed the PFP framework [3], [4], in which the peel-off strategy is introduced. The PFP framework uses the already emerged motor unit firing trains (from FastICA) combined with the least squares method to estimate their waveforms to obtain motor unit action potential trains, and subtracts

Manuscript received 28 January 2024; revised 30 April 2024; accepted 3 May 2024. Date of publication 8 May 2024; date of current version 14 June 2024. This work was supported in part by Shandong Provincial Natural Science Foundation under Grant ZR2021QH053 and in part by Taishan Scholar Project of Shandong Province.

This work involved human subjects or animals in its research. Approval of all ethical and experimental procedures and protocols was granted by the Committee for the Protection of Human Subjects (CPHS) of the University of Texas Health Science Center at Houston, the TIRR Memorial Hermann Hospital, Houston, USA, the Institutional Review Board of Medical College of Wisconsin, Milwaukee, USA, and Northwestern University, Chicago, USA.

The authors are with the School of Rehabilitation Science and Engineering, University of Health and Rehabilitation Sciences, Qingdao, Shandong 266024, China (e-mail: maoqi.chen@uor.edu.cn; dr.ping.zhou@outlook.com).

Digital Object Identifier 10.1109/TNSRE.2024.3398822

them from the raw EMG signal to eliminate their effect on FastICA convergence. Then, FastICA can be iteratively applied on residual signals to continue its searching for new motor unit firing trains. The peel-off strategy has proved to be very effective for overcoming the local convergence of FastICA. This strategy has been followed by recent studies in order to achieve higher decomposition yield [9], [11], [19].

In spite of the strength of the peel-off strategy for high density surface EMG decomposition, successful implementation of the PFP framework largely relies on a series of procedures to overcome the challenges related to peel-off. Given that an ideal waveform estimation is impossible to achieve, unavoidably there will be a difference between the estimated and the real waveforms. Although the differences may be tiny, the caused errors, if not addressed, may accumulate to an extent of compromising the decomposition performance. Therefore, the PFP framework incorporates various complex signal processing strategies, such as constrained FastICA, valley-seeking clustering [20], etc. These efforts work collectively to guarantee the accuracy of waveform estimation and the decomposition performance.

In this study, we set to elucidate the reasons why FastICA tends to fall into local convergence when it is applied for high density surface EMG decomposition. Based on this, we propose a new method and also provide its MATLAB open source code for decomposing high density surface EMG signals. Different from the PFP framework, the novel approach does not apply the peel-off strategy to overcome the local convergence of FastICA but can still achieve comparable decomposition performance. Because the complex signal processing procedures associated with the peel-off strategy are not required any more, the decomposition efficiency can be greatly improved.

II. Rationale and Methodology

A. FastICA

FastICA [5] considers a blind source separation problem described based on the following instantaneous data generation model:

$$\boldsymbol{x} = \boldsymbol{A}\boldsymbol{s} \tag{1}$$

where $\boldsymbol{x} = [x_1, x_2, \cdots, x_m]^T$ is the observed m dimensional random vector. For convenience, $\boldsymbol{x}$ is assumed to be whitened. $\boldsymbol{s} = [s_1, s_2, \cdots, s_n]^T$ is an n dimensional (latent) random vector whose components are assumed mutually independent. Also for convenience, we further assume that $\boldsymbol{s}$ is zero mean. $\boldsymbol{A}$ is the $m \times n$ unknown mixing matrix.

FastICA considers that "nongaussian is independent", and introduces negentropy to measure nongaussianity. To this end, the negentropy maximization criterion is used to find the independent sources from their mixtures. To find one independent source $y = \boldsymbol{w}^T\boldsymbol{x}$ as an estimation of one component of $\boldsymbol{s}$, the decomposition coefficient vector $\boldsymbol{w}$ can be found by solving the following optimization problem:

$$\begin{aligned} max \quad & J(\boldsymbol{w}) = \left[E\left\{G\left(\boldsymbol{w}^T\boldsymbol{x}\right)\right\} - E\{G(v)\}\right]^2 \\ s.t. \quad & h(\boldsymbol{w}) = E\left\{y^2\right\} - 1 = \|\boldsymbol{w}\|_2^2 - 1 = 0 \end{aligned} \tag{2}$$

where $J(\boldsymbol{w})$ is the approximated negentropy using nonpolynomial function G, usually G is chosen as $G(u) = \log\cosh(u)$.v is a standard normal random variable. $h(\boldsymbol{w})$ restricts the variance of output y to be 1, which means that the norm of $\boldsymbol{w}$ is 1 if $\boldsymbol{x}$ is whitened.

The optimal problem can be well solved by the Newton's method. In fact, FastICA is not limited to estimating only one source signal, it is also able to estimate multiple source signals by constraining the orthogonality between the output decomposition coefficient vectors. When estimating the source signals one by one, the deflation version of FastICA is as following [5]:

Assuming that we have got $p-1 (p \geqslant 1)$ decomposition coefficient vectors $\boldsymbol{w}_i, i = 1, 2, \ldots, p-1$, then $\boldsymbol{w}_p$ can be estimated by:

$$\begin{aligned} \boldsymbol{w}_p &\leftarrow E\left\{\boldsymbol{x}G'\left(\boldsymbol{w}_p^T\boldsymbol{x}\right)\right\} - \boldsymbol{w}_p E\left\{G''\left(\boldsymbol{w}_p^T\boldsymbol{x}\right)\right\} \\ \boldsymbol{w}_p &\leftarrow \boldsymbol{w}_p - \sum_{i=1}^{p-1} \boldsymbol{w}_i\left(\boldsymbol{w}_p^T\boldsymbol{w}_i\right) \\ \boldsymbol{w}_p &\leftarrow \boldsymbol{w}_p / \left\|\boldsymbol{w}_p\right\|_2 \end{aligned} \tag{3}$$

There are also symmetric versions of FastICA that can estimate p decomposition coefficient vectors simultaneously:

$$\begin{aligned} &\boldsymbol{w}_i \leftarrow E\left\{\boldsymbol{x}G'\left(\boldsymbol{w}_i^T\boldsymbol{x}\right)\right\} - \boldsymbol{w}_i E\left\{G''\left(\boldsymbol{w}_i^T\boldsymbol{x}\right)\right\}, i = 1, 2, \ldots, p \\ &\boldsymbol{W} \leftarrow \left(\boldsymbol{W}\boldsymbol{W}^{\boldsymbol{T}}\right)^{-1/2}\boldsymbol{W} \end{aligned} \tag{4}$$

where $\boldsymbol{W} = \left[\boldsymbol{w}_1, \boldsymbol{w}_2, \ldots, \boldsymbol{w}_p\right]^T$.

B. Kernel Constrained FastICA

In some cases, certain restrictions need to be placed on the output of FastICA. Now we want y to be uncorrelated to each component in a given q dimensional random vector $\boldsymbol{\phi} = \left[\phi_1, \phi_2, \ldots, \phi_q\right]^T$. Note that when any random variable has a zero mean, "uncorrelated" also implies orthogonality, i.e. we want $E\left\{\phi_i y^T\right\} = 0, i = 1, 2, \cdots, q$.

Considering this problem in the FastICA framework requires solving the following optimization problem:

$$\begin{aligned} max \quad & J(\boldsymbol{w}) = \left[E\left\{G\left(\boldsymbol{w}^T\boldsymbol{x}\right)\right\} - E\{G(v)\}\right]^2 \\ s.t. \quad & h(\boldsymbol{w}) = E\left\{y^2\right\} - 1 = \|\boldsymbol{w}\|_2^2 - 1 = 0 \\ & c_i(\boldsymbol{w}) = E\left\{\phi_i y^T\right\} = 0, i = 1, 2, \ldots, q \end{aligned} \tag{5}$$

It is noted that the optimization problem (5) has q more equality constraints $c_i(\boldsymbol{w})$ than the original FastICA algorithm, so as to limit the orthogonality between the output y and the given random variable ϕ_i.

Although the optimization problem (5) can be solved by the previously proposed constrained FastICA [3], the convergence speed of constrained FastICA is slow, and it is difficult to converge when the number of constraints is large.

Let's consider orthogonal constraints separately. The orthogonal condition means that:

$$E\left\{\boldsymbol{\phi}y^T\right\} = E\left\{\boldsymbol{\phi}\boldsymbol{x}^T\boldsymbol{w}\right\} = E\left\{\boldsymbol{\phi}\boldsymbol{x}^T\right\}\boldsymbol{w} = \boldsymbol{0} \tag{6}$$

Let $\boldsymbol{R}_{\boldsymbol{\phi},\boldsymbol{x}} = E\left\{\boldsymbol{\phi}\boldsymbol{x}^T\right\}_{q\times m}$, equation (6) actually means that $\boldsymbol{w} \in ker\left(\boldsymbol{R}_{\boldsymbol{\phi},\boldsymbol{x}}\right)$, where $ker(\boldsymbol{B}_{q\times m}) = \left\{\boldsymbol{v} \in \mathbb{R}^m \mid \boldsymbol{B}\boldsymbol{v} = \boldsymbol{0}\right\}$ denotes the kernel of a matrix $\boldsymbol{B}$. We further let $\boldsymbol{\Psi}_{m\times b} = \left[\boldsymbol{\psi}_1, \boldsymbol{\psi}_2, \ldots, \boldsymbol{\psi}_b\right]$ to be a matrix consisting of an orthonormal basis $\left\{\boldsymbol{\psi}_1, \boldsymbol{\psi}_2, \ldots, \boldsymbol{\psi}_b\right\}$ of $ker\left(\boldsymbol{R}_{\boldsymbol{\phi},\boldsymbol{x}}\right)$, where $b(\leqslant m)$ is the rank of $ker\left(\boldsymbol{R}_{\boldsymbol{\phi},\boldsymbol{x}}\right)$.

Then $\boldsymbol{w} \in ker\left(\boldsymbol{R}_{\boldsymbol{\phi},\boldsymbol{x}}\right)$ implies there exists a vector $\boldsymbol{\theta} = [\theta_1, \theta_2, \ldots, \theta_b]^T$ satisfying

$$\boldsymbol{w} = \boldsymbol{\Psi}\boldsymbol{\theta} \tag{7}$$

Furthermore, we define a new random vector $\boldsymbol{z}$ by:

$$\boldsymbol{z} = \boldsymbol{\Psi}^T\boldsymbol{x} \tag{8}$$

Substituting Equations (7) and (8) into the optimization problem (5), it is a surprise that the optimization problem (5) becomes the following form:

$$\begin{aligned} max \quad & J_1(\boldsymbol{\theta}) = \left[E\left\{G\left(\boldsymbol{\theta}^T\boldsymbol{z}\right)\right\} - E\{G(v)\}\right]^2 \\ s.t. \quad & h(\boldsymbol{\theta}) = E\left\{y^2\right\} - 1 = \|\boldsymbol{\theta}\|_2^2 - 1 = 0 \end{aligned} \tag{9}$$

It can be seen that the optimization problem (9) is exactly the same as the original FastICA optimization problem (2). The constraints $c_i(\boldsymbol{w}), i = 1, 2, \ldots, q$ are eliminated by already restricting $\boldsymbol{w} \in ker\left(\boldsymbol{R}_{\boldsymbol{\phi},\boldsymbol{x}}\right)$. This means that we only need to transform the observed random vector $\boldsymbol{x}$ into the new vector space using $\boldsymbol{\Psi}^T$, and then the solution of the optimization problem (9) is trivial. This method restricts the search of decomposition vectors in a given kernel space, so we call it kernel constrained FastICA.

C. Correlation Constrained FastICA

In this study, the constrained FastICA method introduced in [3] is also updated. We show that FastICA with cross-correlation constraints can have a more efficient iterative method, without the need to update the Lagrange multipliers and correlation coefficients. To avoid confusion, we refer to this new version as correlation constrained FastICA.

Now consider a problem opposed to kernel constrained FastICA, where we want y, the output of FastICA, to be as correlated as possible with a given reference random variable r, that is, we want $E\left\{ry^T\right\}$ as large as possible. In [3], we used the augmented Lagrange multiplier method to solve this problem. When setting the constraint of cross-correlation, we preset a lower bound of correlation coefficient. However, since the exact lower bound in the final convergence is unknown, we need to update the lower bound gradually in order to ensure convergence in the update process. This may make the constrained FastICA converge slowly. In fact, the Newton's method in FastICA can also be used to deal with this problem, thus greatly increasing the speed of convergence. For whitened observed vector $\boldsymbol{x}$, consider the following problem:

$$\begin{aligned} min \quad & J_2(\boldsymbol{w}) = E\left\{G\left(\boldsymbol{w}^T\boldsymbol{x}\right)\right\} - \mu E\left\{ry^T\right\} \\ s.t. \quad & h(\boldsymbol{w}) = \|\boldsymbol{w}\|_2^2 - 1 = 0 \end{aligned} \tag{10}$$

where G is the same non-polynomial function in (2) (i.e. $G(u) = \log\cosh(u)$). As derived in [5], the maxima of $J(\boldsymbol{w}) = \left[E\left\{G\left(\boldsymbol{w}^T\boldsymbol{x}\right)\right\} - E\{G(v)\}\right]^2$ are obtained at certain optima of $E\left\{G\left(\boldsymbol{w}^T\boldsymbol{x}\right)\right\}$. More specifically, maximizing $\left[E\left\{G\left(\boldsymbol{w}^T\boldsymbol{x}\right)\right\} - E\{G(v)\}\right]^2$ is equivalent to minimizing $E\left\{G\left(\boldsymbol{w}^T\boldsymbol{x}\right)\right\}$ given that our source signals are sparse and super-Gaussian motor unit firing trains. For the sake of simplicity, let's rewrite our objective function into this more concise form. The second term $-\mu E\left\{ry^T\right\}$ in objective function is a penalty term, and the penalty weight μ is a suitable positive constant. Here, we turn the original cross-correlation constraint into a penalty term in the objective function, and consequently, the difficulty of unknown constraint lower bound can be avoided.

Define the Lagrangian function of (10) as:

$$L(\boldsymbol{w}, \beta) = E\left\{G\left(\boldsymbol{w}^T\boldsymbol{x}\right)\right\} - \mu E\left\{ry^T\right\} + \frac{\beta}{2}\left(\|\boldsymbol{w}\|_2^2 - 1\right) \tag{11}$$

where β is the Lagrange multiplier.

According to the Karush-Kuhn-Tucker conditions [21], the optima of (10) are obtained at points where:

$$\nabla_{\boldsymbol{w}} L = E\left\{\boldsymbol{x}G'\left(\boldsymbol{w}^T\boldsymbol{x}\right)\right\} - \boldsymbol{\vartheta}\mu + \boldsymbol{w}\beta = \boldsymbol{0} \tag{12}$$

where $\boldsymbol{\vartheta} = E\left\{\boldsymbol{x}r^T\right\}$. Further, the second derivative of the Lagrangian function can be derived as:

$$\begin{aligned} \nabla_{\boldsymbol{w}}^2 L &= E\left\{\boldsymbol{x}\boldsymbol{x}^T G''\left(\boldsymbol{w}^T\boldsymbol{x}\right)\right\} + \beta\boldsymbol{I} \\ &\approx E\left\{\boldsymbol{x}\boldsymbol{x}^T\right\} \cdot E\left\{G''\left(\boldsymbol{w}^T\boldsymbol{x}\right)\right\} + \beta\boldsymbol{I} \\ &= \left(E\left\{G''\left(\boldsymbol{w}^T\boldsymbol{x}\right)\right\} + \beta\right)\boldsymbol{I} \end{aligned} \tag{13}$$

Here a reasonable approximation is made since $\boldsymbol{x}$ is whitened. Then the following approximative Newton iteration can be obtained:

$$\boldsymbol{w} \leftarrow \boldsymbol{w} - \left[E\left\{G'\left(\boldsymbol{w}^T\boldsymbol{x}\right)\right\} - \boldsymbol{\vartheta}\mu + \boldsymbol{w}\beta\right] / \left[E\left\{G''\left(\boldsymbol{w}^T\boldsymbol{x}\right)\right\} + \beta\right] \tag{14}$$

Because of the normalization constraint of $\boldsymbol{w}$, equation (14) can be simplified as:

$$\boldsymbol{w} \leftarrow \boldsymbol{w}E\left\{G''\left(\boldsymbol{w}^T\boldsymbol{x}\right)\right\} - E\left\{\boldsymbol{x}G'\left(\boldsymbol{w}^T\boldsymbol{x}\right)\right\} + \boldsymbol{\vartheta}\mu \tag{15}$$

Benefiting from the whitened $\boldsymbol{x}$ and the normalization constraint of $\boldsymbol{w}$, the Lagrange multiplier β does not need to be concerned. To this end, the iteration of cross-correlation constrained FastICA is obtained as:

$$\begin{aligned} &\boldsymbol{w} \leftarrow \boldsymbol{w}E\left\{G''\left(\boldsymbol{w}^T\boldsymbol{x}\right)\right\} - E\left\{\boldsymbol{x}G'\left(\boldsymbol{w}^T\boldsymbol{x}\right)\right\} + \boldsymbol{\vartheta}\mu \\ &\boldsymbol{w} \leftarrow \boldsymbol{w}/\|\boldsymbol{w}\|_2 \end{aligned} \tag{16}$$

In general, the convergence rate is not particularly sensitive to the value of the penalty weight μ, as long as it is within a reasonable range. However, μ should not be set very large to make the optimization problem ill-posed.

D. 2CFastICA for High Density Surface EMG Decomposition

Now consider the generative high density surface EMG model. Without causing confusion, $\boldsymbol{x} = [x_1, x_2, \cdots, x_m]^T$ and $\boldsymbol{s} = [s_1, s_2, \cdots, s_n]^T$ are still used to denote the observed

random vector and source vector, respectively. However, the multichannel surface EMG generative model should be described as a convolutional model, specifically for one component of $\boldsymbol{x}$, we have:

$$x_i(t) = \sum_{j=1}^{n} \sum_{\tau=0}^{l-1} a_{ij}(\tau) s_j(t-\tau); i = 1, 2, \ldots, m \quad (17)$$

where x_i is the i th channel of surface EMG signal. a_{ij} stands for the motor unit action potential waveform of j th motor unit in the i th channel, and l is the length of the waveform. The source $s_j(t) = \sum_k \delta\left(t - T_{j,k}\right)$ stands for the j th motor unit firing train, which is a sparse binary random variable (i.e. either 0 or 1) that indicates whether the j th motor unit fires at a specific time t. $T_{j,k}$ is the k th firing time of the j th motor unit, δ represents the discrete-time unit impulse function. Due to the firing properties of motor units, we further assume that $T_{j,k+1} - T_{j,k} > l$.

Note that the convolutional model of equation (17) can actually be rewritten into the form of equation (1), for which FastICA can be used to find the source signal. However, it should be noted that in this case, the source signal includes not only $\boldsymbol{s}$ itself, but also its delays $\boldsymbol{s}(t-\tau)$, $\tau = 1, 2, \ldots, l-1$. Clearly, due to the definition, $\boldsymbol{s}$ and its delays are orthogonal to each other.

In order to facilitate using the FastICA algorithm to separate the convolutional model EMG signal, the signal is usually pre-extended by adding its d-delayed versions. We define the following extended random vector:

$$\widetilde{\boldsymbol{x}}(t) = \left[\boldsymbol{x}^T(t), \boldsymbol{x}^T(t-1), \ldots, \boldsymbol{x}^T(t-d)\right]^T \quad (18)$$

$$\widetilde{\boldsymbol{s}}(t) = \left[\boldsymbol{s}^T(t), \boldsymbol{s}^T(t-1), \ldots, \boldsymbol{s}^T(t-l-d+1)\right]^T \quad (19)$$

Then the extended convolutional model can be expressed by the following matrix multiplication form:

$$\widetilde{\boldsymbol{x}} = \tilde{\boldsymbol{A}}\widetilde{\boldsymbol{s}} \quad (20)$$

where $\widetilde{\boldsymbol{A}}$ is a matrix containing all the waveform coefficients a_{ij} in a proper order (for details, please refer to [1]). Note that the equation (20) is equivalent to equation (17) when the delay factor d is zero. This extension is not necessary, but it is usually recommended because combining the observed random vector $\boldsymbol{x}$ and its delays can achieve an effect analog to FIR filtering. However, appropriate setting of the delay factor d needs to be considered since the extension also increases the computation load and may cause the signal to be ill-conditioned.

In summary, after confirming that the EMG generative model can be expressed in the form of equation (20), FastICA can be applied on model (20) to estimate motor unit firing trains. One should note that in (20), $\tilde{\boldsymbol{s}}$ contains the source $\boldsymbol{s}$ as well as its various delayed versions. Therefore, the output of FastICA will be certain s_i or its delays, and both of them actually correspond to the same motor unit firing train. The original orthogonalization steps in equation (3) or (4) already constrain the different outputs to be orthogonal to each other. However, this strategy does not prevent FastICA from converging to the same motor unit firing train since s_i and its delays are also orthogonal to each other. In other words, to prevent FastICA from converging to the same motor unit firing train, the new estimated firing train should be orthogonal not only to the previously estimated firing trains, but also to their delays.

In fact, it is immediately apparent that this can be easily done using our proposed kernel constrained FastICA algorithm. When estimating a new source signal, we only need to constrain the desired decomposition coefficient vector in the kernel space of the cross-correlation matrix between the identified sources (including their delays) and the observation vector. In addition, to improve the accuracy of the decomposition, it is necessary to refine each estimated motor unit firing train with correlation constrained FastICA. The specific procedures are the same as in [3], that is, for each extracted motor unit firing train, we use it as the reference signal r to drive cross-correlation constrained FastICA to converge to the source component with the maximum cross-correlation with r, and repeat this process until the output of correlation constrained FastICA no longer changes. Due to the cross-correlation constraint, the output of correlation constrained FastICA tends to have a higher signal-to-noise ratio (SNR) than the direct output of FastICA, and therefore any erroneous or missed spikes can be better fixed.

Now we can summarize the new proposed decomposition framework. This framework mainly relies on two improved FastICAs with cross-correlation constraints, i.e. the kernel constrained FastICA and correlation constrained FastICA. Among them, kernel constrained FastICA expects the correlations between the FastICA output and the given random variables to be 0, while correlation constrained FastICA expects the FastICA output to be as correlated as possible with the given reference. Because two constrained FastICA algorithms are key components for the new method, we name it as 2CFastICA for simplicity.

Now we provide the pseudocodes for 2CFastICA (Algorithm 1).

Considering the properties of the non-polynomial function G as well as the cross-correlation function, the penalty weight $\mu = 0.3$ is considered to be a reasonable empirical value in surface EMG decomposition. Note that when constructing the orthogonal constraint vector $\boldsymbol{\phi}$ in the pseudocodes, the delay of the identified source only ranges from $-d$ to d. While theoretically this may not be enough to cover the real delay range in the model (20), practically the duration of the motor unit action potential is not long and the energy is mainly concentrated in the middle part, so this delay range is usually enough to avoid convergence to the same motor units. Note that the desired motor unit firing trains can be extracted from the output source signal $\boldsymbol{s}$, and subsequently, the waveform information of motor unit action potentials is also available by the least squares method (as detailed in the PFP framework [3]).

III. Performance Validation

A. Performance Evaluation Using Simulated EMG

1) Surface EMG Simulation: Surface EMG signals from 5 different motor unit pools were simulated [22]. Each simulated motor unit pool contained 100 motor units whose

Algorithm 1 2CFastICA

Extend (by delay factor d) and whiten the EMG signal $\boldsymbol{x}$ to be $\tilde{\boldsymbol{x}}$. Set count $p \leftarrow 1$.
repeat
  // Kernel Constrained FastICA
  Construct $\boldsymbol{\phi} = \left[\boldsymbol{s}^T(t+d), \boldsymbol{s}^T(t+d-1), ..., \boldsymbol{s}^T(t-d)\right]^T$, where $\boldsymbol{s} = \left[s_1, s_2, ..., s_{p-1}\right]^T$.
  Estimate $\boldsymbol{R}_{\boldsymbol{\phi},\tilde{\boldsymbol{x}}} = E\left\{\boldsymbol{\phi}\tilde{\boldsymbol{x}}^T\right\}$.
  Find an orthonormal basis $\boldsymbol{\Psi}$ of $ker\left(\boldsymbol{R}_{\boldsymbol{\phi},\tilde{\boldsymbol{x}}}\right)$.
  Estimate s_p from $\boldsymbol{\Psi}^T\tilde{\boldsymbol{x}}$ using FastICA.
  // Correlation Constrained FastICA
  Refine s_p by correlation constrained FastICA. Set count $p \leftarrow p+1$.
until no new reliable source can be found.

recruitment characteristics followed the model described in [23]. Motor units were activated in order of the number of muscle fibers they innervated, and motor units with fewer muscle fibers were activated first. The discharge rate range of the motor units was set to $8-35$ Hz. The last motor unit was recruited at 40% maximal excitation. The simulated surface EMG was recorded by a 64-channel surface electrode array (arranged in 8 by 8 channels, with an interelectrode distance of 4 mm for both horizontal and vertical directions). The electrode array was placed with its columns aligned parallel to the muscle fiber direction and its center electrodes located approximately over the innervation zones. The simulated signals were recorded at a sampling rate of 2 kHz per channel. Three excitation levels (3%, 10%, and 45% maximum excitation) were simulated, which corresponded to 29, 62, and 100 active motor units. Each contraction lasted for 10 s. For a 64-channel recording system, the setting of the three excitation levels aimed to examine the performance of 2CFastICA when the number of sources was much less than, close to, and much more than the number of available observations, respectively. For each excitation level, different SNRs ranging from 0, 10, and 20 dB were also simulated with additive zero-mean Gaussian noise (spatially independent). Thus, a total of 45 surface EMG signals were simulated for decomposition performance evaluation (3 excitation levels $\times$ 3 SNR levels $\times$ 5 motor unit pools).

2) Evaluation Results: In order to assess decomposition performance, the decomposition Recall and Precision of a specific identified spike train are defined as follows [3]:

$$\begin{aligned} Recall &= \frac{TP}{TP+FN} \\ Precision &= \frac{TP}{TP+FP} \end{aligned} \tag{21}$$

where TP (true positives) denotes the number of correctly identified spikes, FN (false negatives) is the number of unidentified spikes, and FP (false positives) is the number of misplaced spikes. Before calculating these parameters, the two spike trains for comparison were first aligned using the correlation function method proposed in [3]. After the alignment, two spikes from different spike trains were accepted to be corresponding spikes when they were located within ± 1 ms.

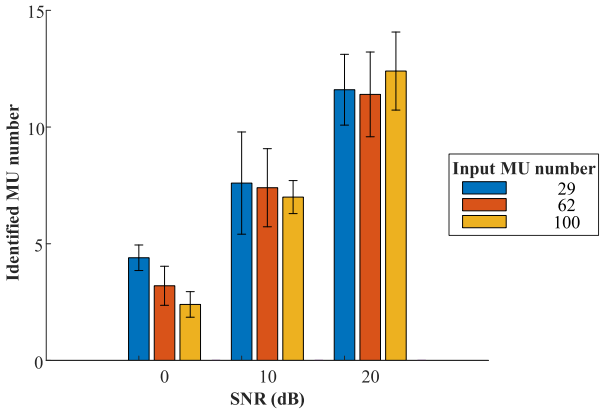

Fig. 1. Average number of identified motor units at different input motor unit numbers and SNR levels.

Then F1-score, the harmonic mean of Recall and Precision, was used as the final measure of decomposition performance:

$$F1 = \frac{2}{\frac{1}{Precision} + \frac{1}{Recall}} \tag{22}$$

The 2CFastICA decomposition method was tested with all the simulated surface EMG signals. Fig. 1 and Fig. 2 summarize the average number of motor units and the average F1-score across different input motor unit numbers and SNR levels, respectively.

B. Two Source Validation Using Intramuscular EMG

1) Dataset Description: In this validation study, the same datasets were used as in the previous two source validation of the PFP framework [24]. The datasets contain 114 trials, and each trial includes a 64-channel high density surface EMG signal and a single channel intramuscular EMG signal, which were simultaneously collected from an isometric contraction at a low-force level of the first dorsal interosseous (FDI) muscle of five neurologically intact subjects and a chronic stroke subject. All subjects gave written informed consent before any experiment procedures. The experimental protocols were approved by the Committee for the Protection of Human Subjects (CPHS) of the University of Texas Health Science Center at Houston and the TIRR Memorial Hermann Hospital (Houston, USA). For details on subject information,

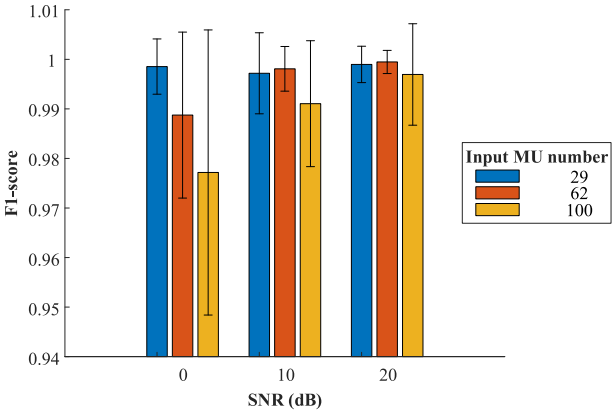

Fig. 2. Average F1-score per reconstructed motor unit at different input motor unit numbers and SNR levels.

the experimental setup, protocols, equipment, and details of intramuscular EMG decomposition, please refer to [24].

2) Evaluation Results: The matching rate (MR) was calculated to measure the matching degree of two spike trains identified from experimental EMG signals. MR is defined as:

$$MR = \frac{2 \cdot N_{COM}}{N_S + N_I} \cdot 100\% \tag{23}$$

where N_S *and* N_I are the total number of the spikes from the surface EMG spike train and the intramuscular EMG spike train, respectively. N_{COM} stands for the number of the common spikes. Consistent with the simulated study, two spikes from different spike trains were accepted as corresponding spikes when they were located within ± 1 ms. Note that if we consider the intramuscular EMG spike train as the "ground-truth spike train", then the MR is indeed a F1-score measure. A common firing train was considered to be identified if the MR $> 80\%$.

An example of two source validation with simultaneous surface and intramuscular EMG recordings is shown in Fig. 3, The top panel shows a 10 s segment of surface EMG signal from one channel of the electrode array. The original signal, the reconstructed signal and the residual signal are shown, respectively, from top to bottom. The bottom panel shows the simultaneously recorded intramuscular EMG signal in the same way. The middle panel shows the firing trains of the identified motor units from the surface EMG and their waveforms in this channel, with the motor units arranged from top to bottom in the order in which they were identified. The third motor unit can be matched to the motor unit identified from the intramuscular EMG with a MR of 99.6%, and the only inconsistent discharge is indicated in red.

Fig. 4 shows the objective function values $(J(x) = [E\{G(x)\} - E\{G(\nu)\}]^2)$ of the decomposition output corresponding to different motor units in this example (arranged in their order of identification). The green shaded part in the bottom is the range of function values corresponding to each channel of the EMG signal. As mentioned in the method section, the value of the objective function $J(x)$ actually represents the nongaussianity of the random variable x. Therefore, in general, motor unit spike trains with larger nongaussianity are preferentially decomposed.

Among all 114 trials data, the length of segments used for decomposition analysis varied from 10 s to 70 s (34.1 ± 8.9 s). Overall, a total of 956 (on average 6.4 ± 2.9 per trial) motor units were identified from the high density surface EMG signals using the 2CFastICA method. A total of 217 (on average 1.9 ± 1.0 per trial) motor units were identified from the intramuscular EMG. A total of 170 motor units were accepted as common ones. An average MR for the common motor units was $(97.2 \pm 3.5)\%$. Fig. 5 shows the histogram of MRs of all the random pairs within each of the 114 trials. Similar to the results in [24], the distribution of MRs presents a bimodal pattern.

C. Two Source Validation Using ALS Data

1) Dataset Description: We also conducted a different form of two-source validation taking advantages of the high density surface EMG characteristics of patients with amyotrophic lateral sclerosis (ALS) as described previously [25]. A total of 22 trials of 64-channel high density surface EMG data were used. They were collected from the FDI muscle of 9 subjects with the diagnosis of definite ALS or probable ALS with Laboratory Support (El Escorial criteria [26]). The study was approved by the Institutional Review Board of Medical College of Wisconsin (Milwaukee, USA) and Northwestern University (Chicago, USA), and all the subjects gave their written consent. The different channels of each trial were grouped into two datasets, i.e. the interference dataset and the sparse dataset. The interference dataset only contained those channels with high levels of motor unit action potential superposition while the sparse dataset only contained those channels capturing distinguishable motor units (most likely due to motor unit loss and muscle fiber reinnervation), readily discriminated through visual inspection or routine clustering algorithms. For details on subject information, the experimental setup, protocols, equipment, and details of sparse dataset decomposition, please refer to [25].

2) Evaluation Results: Similar to two-source validation using intramuscular EMG, the MR defined in Equation (23) was used to measure the matching degree of the motor unit spike trains independently identified from the sparse dataset and the interference dataset, note that in this context N_S *and* N_I represent the number of spikes (of the spike train) identified from the sparse dataset and interference dataset, respectively, N_{COM} stands for the number of common spikes.

Fig. 6 shows an example of the validation process, where the top panel is the selected channels from the interference dataset, the middle panel is the firing instants of the identified motor units by applying 2CFastICA to the interference dataset, and the bottom panel shows two channels from the sparse dataset. In this example, the interference dataset contains 14 channels and for clarity only three channels are shown in the figure. It was straightforward to extract two different motor units from the two channels of the sparse dataset by visual inspection of the action potential amplitude and waveform information. These two motor units (indicated by red and blue bars, respectively) were also obtained by applying 2CFastICA to the 14 channels of the interference dataset. The

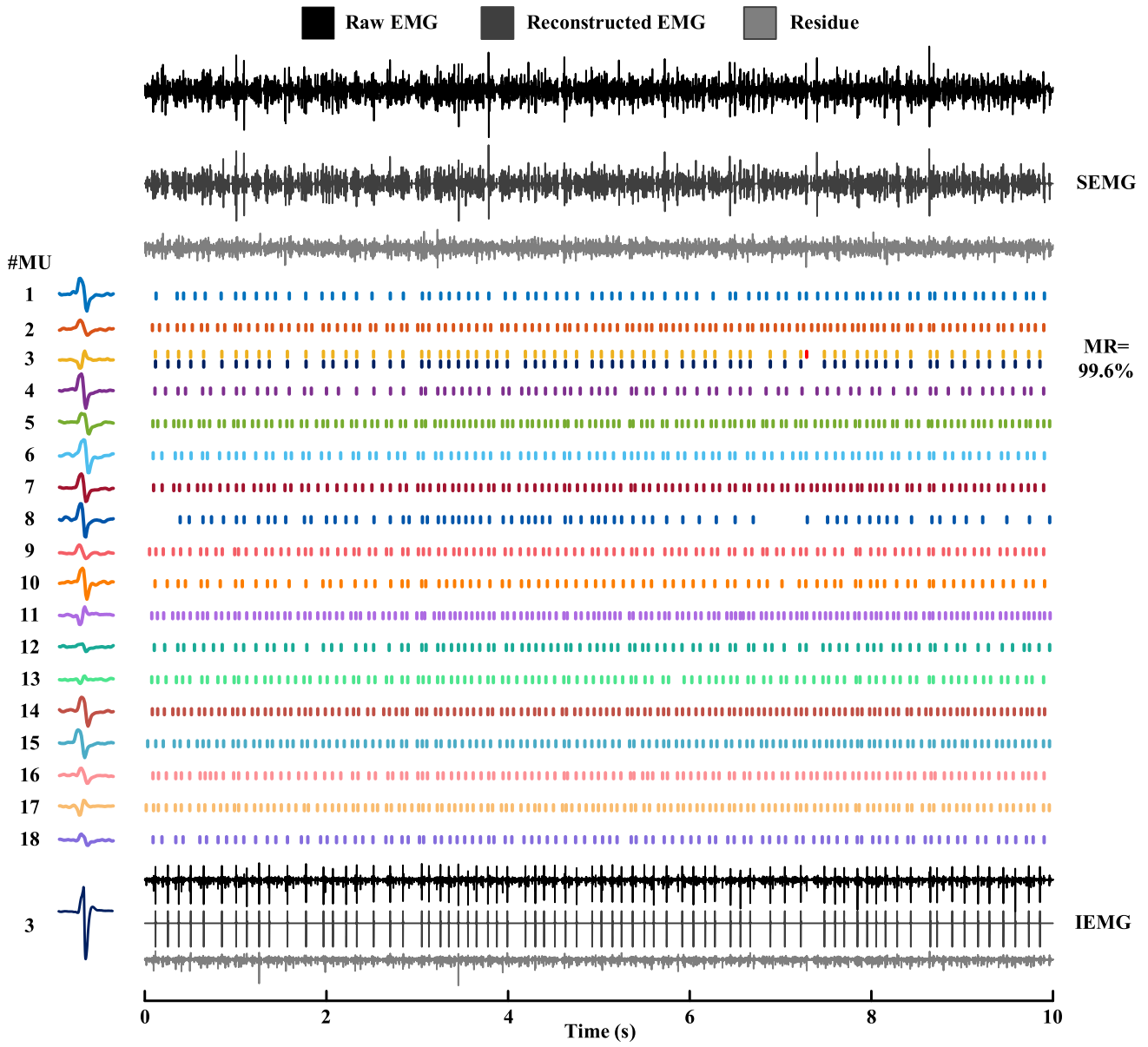

Fig. 3. An example of discharge timing comparison for motor units identified from simultaneously collected surface and intramuscular EMG signals.

firing instants of these two common motor units from the interference dataset and the sparse dataset matched very well, as shown in the figure, where the same color (red or blue) was used to represent the common motor units.

As suggested by the objective function values of this example in Fig. 7, the nongaussianity of the sparse dataset is generally higher than that of the interference dataset. The objective function values of some channels in the sparse set are even higher than the decomposition result of the interference dataset (so these channels can be easily decomposed and used for the performance evaluation purpose).

Overall, the number of channels in the interference dataset was 42.6% of the total number of channels. A total of 140 (on average 6.4 $\pm$ 2.9 per trial) motor units were identified from the interference dataset using 2CFastICA and a total of 34 (on average 1.5 $\pm$ 0.5 per trial) motor units were identified from the sparse dataset. Notably, all the 34 motor units from the sparse dataset were also identified as common ones, with an average MR of $(99.4 \pm 0.9)\%$.

IV. Discussion

This study presents a novel deflationary high density surface EMG decomposition framework. The framework focuses on solving the local convergence problem of FastICA and improving the efficiency and accuracy of high density surface EMG decomposition. Given that FastICA always falls into local optima, our previously developed PFP framework introduced a peel-off strategy to overcome the local convergence of FastICA [3], [4]. Specifically, the motor unit action potential trains of identified motor units from FastICA are estimated by the least squares method, and progressively subtracted from the original surface EMG signals (through an iterative processing) to reduce their influence on the convergence of FastICA. Although this strategy has proven to be very

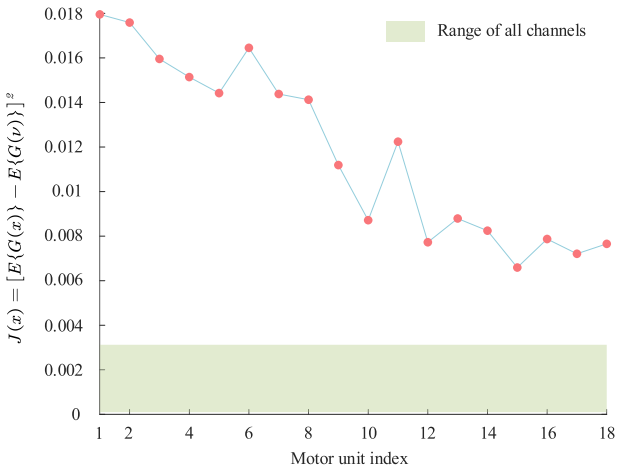

Fig. 4. The objective function values of different identified motor unit spike trains in the example of Fig. 3.

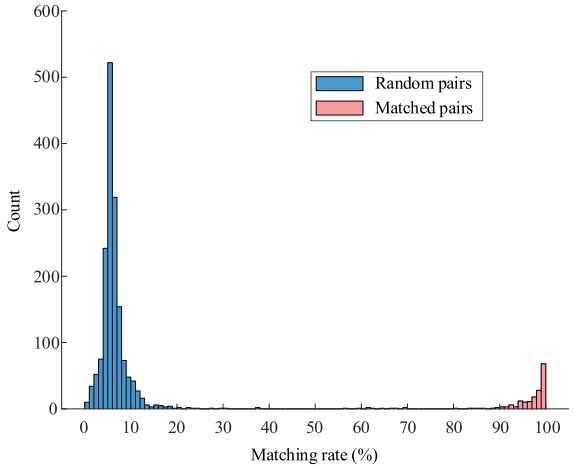

Fig. 5. Distribution of MRs between random pairs of surface and intramuscular motor unit firing trains in individual trials.

effective, unfortunately it also potentially creates several problems. For example, the discrepancies of the motor unit action potential waveform estimation may affect the accuracy of the decomposition results. In addition, the iterative peel-off processing slows down the efficiency, particularly when the signal duration is long. In this study, we found that in fact, the local convergence problem of FastICA can be solved by only using the kernel space constraint without peel-off. This is a much more efficient solution than the peel-off strategy and meanwhile greatly improves the SNR (and thus accuracy) of the FastICA output.

The novel method proposed in this study is named as 2CFastICA because it involves kernel constrained FastICA and correlation constrained FastICA, which complement each other in high density surface EMG decomposition. Firstly, kernel constrained FastICA solves the local convergence problem of FastICA in a very efficient way, so that the motor units can be estimated one by one, without requiring the previous peel-off strategy. Secondly, correlation constrained FastICA is used to further refine the output of kernel constrained FastICA and correct possible erroneous or missed spikes, thus warranting the reliability of decomposition results. Meanwhile, the efficiency of kernel constrained FastICA can also be revealed by the fact that the SNR of the output of kernel constrained FastICA is usually higher than that from the peel-off strategy, so that correlation constrained FastICA can converge with fewer iterations. Based on Newton's method, both of the constrained FastICAs inherit the advantages of fast convergence of FastICA, thus greatly improve the decomposition efficiency. With the kernel space gradually compressed, the algorithm can dig out almost all possibly decomposable motor units under the convolutional mixture model.

Assessment of decomposition performance is essential for any newly developed EMG decomposition method. Common assessment approaches include surface EMG simulation and testing with experimental surface EMG signals. Both approaches were implemented in this study to evaluate the performance of 2CFastICA. For the experimental approach, although 2CFastICA was tested with considerable experimental high density surface EMG signals from weak to strong contractions, we chose to only report the results from two-source validation experimental signals, given that the composition is not known *a priori* in a real or experimental EMG signal, and two-source signals provide a useful and widely recognized approach to quantifying the decomposition performance by cross-checking the timing information (i.e. agreement on the timing) of the common motor unit discharges [24], [27], [28]. In addition to the conventional two-source validation typically involving simultaneous surface EMG and intramuscular EMG recordings, a different two-source validation method was also performed, taking advantage of the surface EMG characteristics of ALS patients and the spatial recording capacity of an electrode array [25].

It is noted that the results of the two-source validation were very similar for 2CFastICA and PFP. For example, in the two-source validation using intramuscular EMG, PFP achieved a performance of an average of 7.6 ± 2.7 motor units per trial, a total of 168 common motor units, and an average MR of 96.8%, from the same datasets [24]. Compared with the results of the current study, there was no remarkable difference in performance evaluation between the two algorithms. However, it is interesting to observe that PFP found common motor units in all 114 trials, while 2CFastICA failed to identify common motor units in four trials although it found more common motor units than PFP. Although such a difference did not have a notable influence on the overall decomposition performance, it implies that there might be somewhat different mechanisms acting on FastICA convergence between the peel-off strategy and the kernel constraint. Understanding this mechanism difference may help further increase the decomposition yield. It is also worth to note the bimodal distribution of MRs for both PFP and 2CFastICA. This indicates that two randomly matched motor unit firing trains either matched very well or did not match at all. As previously discussed in [29], caution is required for the presence of intermediate MRs of two spike trains, which may suggest less reliable decomposition.

In the two-source validation using intramuscular EMG, the final decomposition MR of 2CFastICA only improved by about 0.4% on average compared with PFP. This is not surprising since the average MR of PFP is already as high as

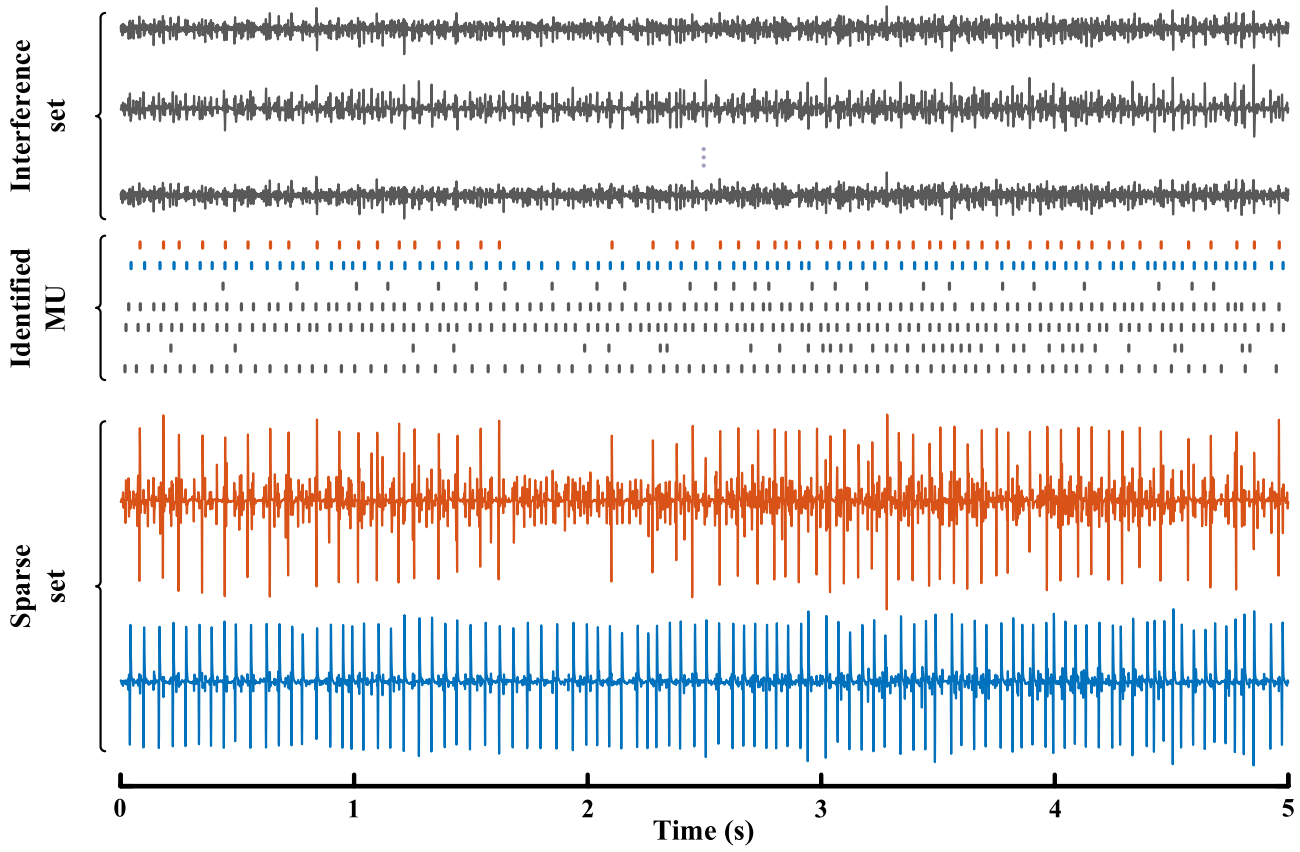

Fig. 6. A demonstration of the two-source validation using ALS data (please see text for details).

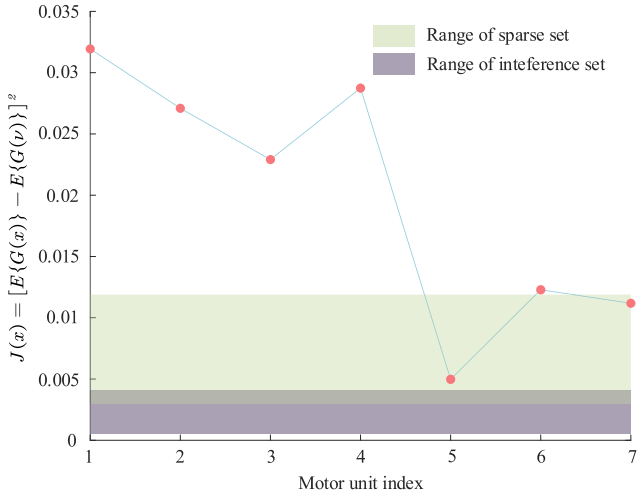

Fig. 7. The objective function values of different identified motor unit spike trains in the example of Fig. 6.

96.8%. However, if viewed from another perspective, these results also indicate that in the previous PFP framework, the peel-off processing does not cause a noticeable drop in decomposition accuracy. This is because the constrained FastICA serves as a powerful error correction mechanism, a key design in the PFP decomposition framework. In other words, even the peel-off step may introduce some errors to the FastICA output, most of these errors can be corrected by the followed constrained FastICA. We note that Negro et al. commented that the peel-off strategy may decrease the accuracy of FastICA [6]. In our opinion, this phenomenon, if observed in their practice, may have been attributed to two reasons. Firstly, the error correction mechanism similar to constrained FastICA was lacking, thus the errors caused by the peel-off step could not be fixed. Secondly, the spike triggered averaging was used to estimate the action potential waveforms of the identified motor units, so that the waveform estimation of different motor units was carried out independently, without using all the available information. This limitation was likely to result in relatively large errors, particularly in the case of heavy superposition.

To this end, it can be seen that while the peel-off step is designed to solve the local convergence problem of FastICA in the PFP framework, indeed the constrained FastICA is the core processing that ensures the reliability of the final result. For this reason, the constrained FastICA (actually, a more efficient iteration of constrained FastICA) is still retained as a key component in this study. It is worth noting that compared with the peel-off strategy, the new design of 2CFastICA also provides a more favorable approach towards implementing online high density surface EMG decomposition for real time applications.

Although the peel-off strategy is not needed in the newly developed 2CFastICA method, some components in the previous PFP framework can still be useful. For example, when it is difficult to distinguish between different motor unit spikes with only a simple threshold, valley-seeking clustering [20] can be applied to overcome the difficulty. The useful components of PFP, if needed, can be naturally embedded

into the new framework to facilitate the decomposition performance.

V. Conclusion

This study presents a novel high density surface EMG decomposition method called 2CFastICA, incorporating kernel constrained FastICA and correlation constrained FastICA. The former focuses on overcoming the local convergence of FastICA without requiring the previous peel-off strategy. The latter further refines the output of kernel constrained FastICA to warrant the decomposition accuracy. The performance of applying 2CFastICA for high density surface EMG decomposition was validated by both model-based simulation and experimental two source validation studies. The MATLAB open source code of 2CFastICA is provided (see Appendix).

Appendix: Open Source Code

The MATLAB open source code of 2CFastICA for high density surface EMG decomposition can be found at (https://github.com/maoqichen/High-density-surface-EMG-decomposition-by-2CFastICA). The code is free to download and use for research and non-commercial purposes only.

References

[1] A. Holobar and D. Zazula, "Multichannel blind source separation using convolution kernel compensation," *IEEE Trans. Signal Process.*, vol. 55, no. 9, pp. 4487–4496, Sep. 2007.

[2] A. Holobar and D. Zazula, "Gradient convolution kernel compensation applied to surface electromyograms," in *Proc. Int. Conf. Independ. Compon. Anal. Signal Separat.* Berlin, Germany: Springer, 2007, pp. 617–624.

[3] M. Chen and P. Zhou, "A novel framework based on FastICA for high density surface EMG decomposition," *IEEE Trans. Neural Syst. Rehabil. Eng.*, vol. 24, no. 1, pp. 117–127, Jan. 2016.

[4] M. Chen, X. Zhang, X. Chen, and P. Zhou, "Automatic implementation of progressive FastICA peel-off for high density surface EMG decomposition," *IEEE Trans. Neural Syst. Rehabil. Eng.*, vol. 26, no. 1, pp. 144–152, Jan. 2018.

[5] A. Hyvarinen, "Fast and robust fixed-point algorithms for independent component analysis," *IEEE Trans. Neural Netw.*, vol. 10, no. 3, pp. 626–634, May 1999.

[6] F. Negro, S. Muceli, A. M. Castronovo, A. Holobar, and D. Farina, "Multi-channel intramuscular and surface EMG decomposition by convolutive blind source separation," *J. Neural Eng.*, vol. 13, no. 2, Apr. 2016, Art. no. 026027.

[7] Y. Wen, S. Avrillon, J. C. Hernandez-Pavon, S. J. Kim, F. Hug, and J. L. Pons, "A convolutional neural network to identify motor units from high-density surface electromyography signals in real time," *J. Neural Eng.*, vol. 18, no. 5, Oct. 2021, Art. no. 056003.

[8] C. Chen, S. Ma, Y. Yu, X. Sheng, and X. Zhu, "Segment-wise decomposition of surface electromyography to identify discharges across motor neuron populations," *IEEE Trans. Neural Syst. Rehabil. Eng.*, vol. 30, pp. 2012–2021, 2022.

[9] C. Chen, S. Ma, X. Sheng, and X. Zhu, "A peel-off convolution kernel compensation method for surface electromyography decomposition," *Biomed. Signal Process. Control*, vol. 85, Aug. 2023, Art. no. 104897.

[10] H. Zhao, X. Zhang, M. Chen, and P. Zhou, "Online decomposition of surface electromyogram into individual motor unit activities using progressive FastICA peel-off," *IEEE Trans. Biomed. Eng.*, vol. 71, no. 1, pp. 160–170, Jan. 2024.

[11] Y. Zheng et al., "High-density surface EMG decomposition by combining iterative convolution kernel compensation with an energy-specific peel-off strategy," *IEEE Trans. Neural Syst. Rehabil. Eng.*, vol. 31, pp. 3641–3651, 2023.

[12] H. Zhao, X. Zhang, M. Chen, and P. Zhou, "Adaptive online decomposition of surface EMG using progressive FastICA peel-off," *IEEE Trans. Biomed. Eng.*, vol. 71, no. 4, pp. 1257–1268, Apr. 2024.

[13] C. Dai and X. Hu, "Independent component analysis based algorithms for high-density electromyogram decomposition: Systematic evaluation through simulation," *Comput. Biol. Med.*, vol. 109, pp. 171–181, Jun. 2019.

[14] Y. Ning, N. Dias, X. Li, J. Jie, J. Li, and Y. Zhang, "Improve computational efficiency and estimation accuracy of multi-channel surface EMG decomposition via dimensionality reduction," *Comput. Biol. Med.*, vol. 112, Sep. 2019, Art. no. 103372.

[15] M. R. Mohebian, H. R. Marateb, S. Karimimehr, M. A. Mañanas, J. Kranjec, and A. Holobar, "Non-invasive decoding of the motoneurons: A guided source separation method based on convolution kernel compensation with clustered initial points," *Frontiers Comput. Neurosci.*, vol. 13, p. 14, Apr. 2019.

[16] A. K. Clarke et al., "Deep learning for robust decomposition of high-density surface EMG signals," *IEEE Trans. Biomed. Eng.*, vol. 68, no. 2, pp. 526–534, Feb. 2021.

[17] V. Glaser and A. Holobar, "Motor unit identification from high-density surface electromyograms in repeated dynamic muscle contractions," *IEEE Trans. Neural Syst. Rehabil. Eng.*, vol. 27, no. 1, pp. 66–75, Jan. 2019.

[18] Y. Zheng and X. Hu, "Real-time isometric finger extension force estimation based on motor unit discharge information," *J. Neural Eng.*, vol. 16, no. 6, Oct. 2019, Art. no. 066006.

[19] J. Lundsberg, A. Björkman, N. Malesevic, and C. Antfolk, "Compressed spike-triggered averaging in iterative decomposition of surface EMG," *Comput. Methods Programs Biomed.*, vol. 228, Jan. 2023, Art. no. 107250.

[20] C. Zhang, X. Zhang, M. Q. Zhang, and Y. Li, "Neighbor number, valley seeking and clustering," *Pattern Recognit. Lett.*, vol. 28, no. 2, pp. 173–180, Jan. 2007.

[21] W. Karush, "Minima of functions of several variables with inequalities as side constraints," M.Sc. dissertation. Dept. Math., Univ. Chicago, Chicago, IL, USA, 1939.

[22] D. Farina, L. Mesin, S. Martina, and R. Merletti, "A surface EMG generation model with multilayer cylindrical description of the volume conductor," *IEEE Trans. Biomed. Eng.*, vol. 51, no. 3, pp. 415–426, Mar. 2004.

[23] A. J. Fuglevand, D. A. Winter, and A. E. Patla, "Models of recruitment and rate coding organization in motor-unit pools," *J. Neurophysiol.*, vol. 70, no. 6, pp. 2470–2488, Dec. 1993.

[24] M. Chen, X. Zhang, Z. Lu, X. Li, and P. Zhou, "Two-source validation of progressive FastICA peel-off for automatic surface EMG decomposition in human first dorsal interosseous muscle," *Int. J. Neural Syst.*, vol. 28, no. 9, Nov. 2018, Art. no. 1850019.

[25] M. Chen, X. Zhang, and P. Zhou, "A novel validation approach for high-density surface EMG decomposition in motor neuron disease," *IEEE Trans. Neural Syst. Rehabil. Eng.*, vol. 26, no. 6, pp. 1161–1168, Jun. 2018.

[26] B. R. Brooks, R. G. Miller, M. Swash, and T. L. Munsat, "El escorial revisited: Revised criteria for the diagnosis of amyotrophic lateral sclerosis," *Amyotrophic Lateral Sclerosis Other Motor Neuron Disorders*, vol. 1, no. 5, pp. 293–299, Jan. 2000.

[27] B. Mambrito and C. J. De Luca, "A technique for the detection, decomposition and analysis of the EMG signal," *Electroencephalogr. Clin. Neurophysiol.*, vol. 58, no. 2, pp. 175–188, Aug. 1984.

[28] H. R. Marateb, K. C. McGill, A. Holobar, Z. C. Lateva, M. Mansourian, and R. Merletti, "Accuracy assessment of CKC high-density surface EMG decomposition in biceps femoris muscle," *J. Neural Eng.*, vol. 8, no. 6, Oct. 2011, Art. no. 066002.

[29] M. Chen and P. Zhou, "Caution is necessary for acceptance of motor units with intermediate matching in surface EMG decomposition," *Frontiers Neurosci.*, vol. 16, May 2022, Art. no. 876659.